remote sensing

MDPI

Article

Attitude Determination with GPS L1/Galileo E1 Observations from Common-Clock Receiver: A Comparison of Four Different Models

Mingkui Wu [1,2], Jiahang Li [1], Shuai Luo [3] and Wanke Liu [3,4,*]

[1] School of Geography and Information Engineering, China University of Geosciences (Wuhan), Wuhan 430074, China
[2] Key Laboratory for Digital Land and Resources of Jiangxi Province, East China University of Technology, Nanchang 330013, China
[3] School of Geodesy and Geomatics, Wuhan University, Wuhan 430079, China
[4] Key Laboratory of Geospace Environment and Geodesy, Ministry of Education, Wuhan University, Wuhan 430079, China
* Correspondence: wkliu@sgg.whu.edu.cn

Abstract: The development of the commercial multi global navigation satellite system (GNSS) dual (multi)-antenna common-clock receiver that uses time-synchronization technology has brought new opportunities for high-precision GNSS-based attitude determination. In this article, for the first time, we present a performance comparison of global positioning system (GPS) L1/Galileo navigation satellite system (Galileo) E1 attitude determination with a common-clock receiver using four different models, i.e., the loosely combined single-differenced (SD-LC) model, the tightly combined single-differenced (SD-TC) model, the loosely combined double-differenced (DD-LC) model, and the tightly combined double-differenced (DD-TC) model. We first introduce the SD-LC, SD-TC, DD-LC, and DD-TC relative positioning models with GPS L1/Galileo E1 observations from a common-clock receiver. Then, we present a performance comparison of the four models in both single-epoch and multi-epoch modes using static data collected with a Trimble BD992 common-clock receiver in terms of the ambiguity dilution of precision (ADOP), the ambiguity resolution (AR) success and failure rates, and the positioning and attitude determination accuracy. In the case of the single-epoch mode, the experimental results revealed that the results of the single-differenced (SD) models were identical to those of double-differenced (DD) models, i.e., the results of SD-LC and SD-TC models were identical to DD-LC and DD-TC models, respectively. Moreover, compared with the loosely combined model (SD-LC/DD-LC), the tightly combined model (SD-TC/DD-TC) delivered a much higher AR success rate and a lower AR failure rate, especially under a high elevation cutoff angle. The AR success rate increased by approximately 35.1% under a 40° elevation cutoff angle, while the AR failure rate decreased by approximately 4.3%. In the case of the multi-epoch mode, the experimental results confirmed the advantages of the tightly combined model over the loosely combined model as well as the SD model over the DD model. Compared with the DD-LC and SD-LC models, the AR success rates of the DD-TC and SD-TC models were improved by approximately 16.7% and 0.6% under a 45° elevation cutoff angle, respectively. The AR failure rates were reduced by approximately 12.4% and 0.3%, respectively. Moreover, compared with the DD-LC and DD-TC models, the AR success rates of the SD-LC and SD-TC models under a 45° elevation cutoff angle were improved by approximately 24.0% and 7.9%, respectively, and the AR failure rates were reduced by approximately 19.9% and 7.8%, respectively. Meanwhile, compared with the DD model, the SD model delivered comparable yaw accuracy and remarkably better pitch accuracy. The pitch accuracy was improved by approximately 65.2–75.0%.

Keywords: GNSS attitude determination; common-clock receiver; GPS; Galileo; single-differenced model; double-differenced model

Citation: Wu, M.; Li, J.; Luo, S.; Liu, W. Attitude Determination with GPS L1/Galileo E1 Observations from Common-Clock Receiver: A Comparison of Four Different Models. *Remote Sens.* **2022**, *14*, 5438. https://doi.org/10.3390/rs14215438

Academic Editors: Kejie Chen, Rui Tu and Wei Qu

Received: 31 August 2022
Accepted: 27 October 2022
Published: 29 October 2022

1. Introduction

Global navigation satellite system (GNSS)-based attitude determination can provide real-time three-dimensional attitude information (including yaw, pitch, and roll) for land, sea, air, and space moving vehicles. Because of its advantages of long-term stability, no error accumulation, low cost, light weight, small size, and easy maintenance over traditional inertial navigation system (INS) sensors [1–3], GNSS-based attitude determination has broad prospects in both military and civilian use, such as intelligent transportation, precision agriculture, high-precision surveying and mapping, navigation, aviation, etc.

In GNSS-based attitude determination, the prerequisite for obtaining the high-precision attitude of a vehicle is first obtaining the high-precision baseline vectors between the rigidly mounted antennas using the short-baseline precise relative positioning technology. The double-differenced (DD) model can eliminate or largely reduce the common errors in the satellite, receiver, and signal propagation path and retain the integer nature of ambiguities. It has therefore been widely used in GNSS-based attitude determination [4–7].

When multiple GNSS systems are combined, there are two types of DD models, i.e., the loosely combined DD (DD-LC) model and the tightly combined DD (DD-TC) model. The DD-LC model is generally used due to its simplicity. In the DD-LC model, a reference satellite is selected for each GNSS system separately and only intra-system DD observations are created. These intra-system DD observations of each GNSS system are functionally independent, and the only common parameter among the involved GNSS systems is the baseline vector. In the DD-TC model, however, a single reference satellite is selected for all the involved GNSS systems, and both inter-system and intra-system DD observations are created. The extra link brought by the inter-system DD observations strengthens the adjustment model [8]. With the development of modernized GNSS systems, the Galileo navigation satellite system (Galileo), BeiDou global navigation satellite system (BDS-3), Quasi-Zenith Satellite System (QZSS), and Indian Regional Navigation Satellite System (IRNSS) were designed to transmit navigation signals that overlap with the global positioning system (GPS) (e.g., GPS L1/E1, Galileo E1/E5a, BDS-3 B1C/B2a, QZSS L1/L5, and IRNSS L5) to enhance the compatibility and interoperability between them [9–12]. This creates an advantageous condition for the use of the DD-TC model. Previous studies have revealed that, compared with the DD-LC model, the DD-TC model provides improved performance of ambiguity resolution and precise relative positioning, especially when the observed satellites in each GNSS system are limited and only single-frequency observations are used [13–20]. However, the prerequisite is that the between-receiver differential inter-system bias (DISB) in the DD-TC model is carefully considered. Previous studies have revealed that the DISB between the overlapping frequencies of multi-GNSS systems is close to zero when the involved receivers are of the same type but are generally non-zero with different receiver types [11–14,21]. Since the DISBs are stable in the time domain even though the receiver restarts, they are usually calibrated and corrected in advance [8–14]. In order to solve the problem of rank deficiency caused by the linear correlation between the phase DISB and inter-system DD ambiguities, Tian et al. proposed a particle-filter-based real-time phase DISB estimation approach, which can achieve a real-time, fast, and accurate estimation of phase DISB without prior information or adding additional DISB parameters in the mathematical model [22,23]. Peng et al. further presented a maximum ratio principle-based DISB estimation approach [24]. Shang et al. proposed a state optimal estimation-based DISB estimation approach for multi-GNSS inter-system positioning in complex environments, and the results revealed the advantage of the step-by-step particle-filter-based method [25].

In recent years, the rapid development of commercial dual (multi)-antenna common-clock GNSS receivers that use time-synchronization technology offers a kind of possibility for GNSS-based attitude determination with a single-differenced (SD) model. With such a common-clock receiver, the received GNSS signals from dual (multi)-antennas that connected to the receiver are mixed with the same oscillator. This means that the GNSS observations from the dual (multi)-antennas share the same clock. Therefore, the receiver

clock errors for both the master antenna (or reference station) and slave antennas (or rover stations) are identical and can be eliminated with only the SD model [26,27]. Previous publications have revealed that the SD model with a common-clock receiver could solve the well-known problem encountered in the DD model, i.e., the achievable baseline accuracy in the vertical component is two to three times inferior to the horizontal component. Compared with the DD model, the SD model provides improved baseline accuracy in the vertical component to nearly the same level as the horizontal component. The pitch accuracy is therefore significantly improved to nearly the same level as yaw [28–33]. However, the prerequisite is that the additional line bias (LB) in the SD model, which is composed of the initial phase bias in the receiver and hardware delays from the antennas, receiver, and cables [29,33], should be properly handled in real time. The critical feature of LB includes two aspects: (1) when cables of the same length are used, the phase and code LBs are relatively stable during a short continuous observation period (generally within approximately one day) once the involved common-clock receiver is started, and (2) the phase LBs are linearly correlated with the SD ambiguities [33]. In order to solve the problem of linear correlation between the phase LBs and SD ambiguities, the parameter reorganization method is usually performed, in which one reorganizes the phase LB and SD ambiguities and estimates the lumped phase LB over time with a time-constant or random walk process model [32,33]. An alternative approach is a two-step method in which one first calculates and filters the phase LB over time and then corrects it with the SD model [34,35]. In addition, Macias-Valadez et al. calibrated the phase LB in real time using dedicated hardware devices [36]. Recently, Wu et al. extended the particle filter approach for real-time phase LB estimation, considering that the phase LB has characteristics similar to the phase DISB [37].

In the SD model, the parameter reorganization method is generally performed separately within the SD observations of each GNSS system and is referred to as the loosely combined SD (SD-LC) model in this article. Previous researchers have found that for the overlapping frequencies shared by different GNSS systems their LBs are identical, and thus they can be simply treated as if they are from one constellation in the SD model [33]. This provides the possibility of using the tightly combined SD (SD-TC) model, in which the parameter reorganization is also performed between SD observations between different GNSS systems. Moreover, for the common-clock receiver, the master and rover receivers are of the same type. The DISB between the overlapping frequency of different GNSS systems is therefore close to zero and can be neglected [10–14]. As a consequence of this, the DD-TC model can be easily applied between the overlapping frequencies of different GNSS systems when the common-clock receiver is used.

In this contribution, for the first time, we present a performance comparison of GNSS -based attitude determination with a common-clock receiver using the SD-LC, SD-TC, DD-LC, and DD-TC models. Without a loss of generality, the GPS L1/Galileo E1 observations are used as a representative example. We first deduced the SD-LC, SD-TC, DD-LC, and DD-TC relative positioning models with the GPS L1/Galileo E1 observations from the common-clock receiver. Then, we present a performance assessment of the four models from the aspects of the ambiguity dilution of precision (ADOP), the ambiguity resolution (AR) success and failure rates, and the positioning and attitude accuracy using static short-baseline data collected with a Trimble BD992 dual-antenna common-clock receiver.

2. Relative Positioning Models with GPS L1/Galileo E1 Observations from Common-Clock Receiver

This section introduces the SD-LC, SD-TC, DD-LC, and DD-TC models with common-clock GPS L1/Galileo E1 observations. Considering that only the short baseline is involved in GNSS-based attitude determination, the residual ionospheric and tropospheric errors can be ignored and thus will be not presented in the following formulas for simplicity. Moreover, for the common-clock receiver, although the receiver clock errors are eliminated by the SD model, additional code and phase LBs are introduced and should be considered.

Assuming that both the master antenna, k, and slave antenna, l, that connected to a common-clock receiver simultaneously track n_G GPS satellites and n_{E} Galileo satellites at the overlapping L1/E1 frequency, the GPS L1/Galileo E1 SD observation equation with a common-clock receiver is represented by [33]:

$$\begin{aligned}
\Delta P_{kl,L1}^{i_G} &= \Delta\rho_{kl}^{i_G} + \alpha_{kl,L1}^{G} + \Delta\varepsilon_{kl,L1}^{i_G} \\
\Delta\varphi_{kl,L1}^{i_G} &= \Delta\rho_{kl}^{i_G} + \lambda_{L1}\cdot\left(\beta_{kl,L1}^{G} + N_{kl,L1}^{i_G}\right) + \Delta e_{kl,L1}^{i_G} \\
\Delta P_{kl,E1}^{j_E} &= \Delta\rho_{kl}^{j_E} + \alpha_{kl,E1}^{E} + \Delta\varepsilon_{kl,E1}^{j_E} \\
\Delta\varphi_{kl,E1}^{j_E} &= \Delta\rho_{kl}^{j_E} + \lambda_{E1}\cdot\left(\beta_{kl,E1}^{E} + \Delta N_{kl,E1}^{j_E}\right) + \Delta e_{kl,E1}^{j_E}
\end{aligned} \tag{1}$$

where Δ is the between-receiver SD operator, $i_G = 1_G, 2_G, 3_G, \cdots, n_G$, $j_E = 1_E, 2_E, 3_E, \cdots, n_E$, subscripts $L1$ and $E1$ denote the GPS L1 and Galileo E1 frequencies, respectively, and the corresponding wavelengths are λ_{L1} and λ_{E1} ($\lambda_{L1} = \lambda_{E1}$); P and φ are the code and phase observations in meters, respectively; ρ is the geometric distance between the satellite and antenna; α is the code LB; β is the phase LB, which is composed of the SD initial phase bias and SD phase hardware delay; N is integer ambiguity; and ε and e are the code and phase noise, respectively.

2.1. SD-LC Model

In Equation (1), the phase LBs are linearly correlated with the SD ambiguities, which will lead to the rank deficiency of the normal equation. As a consequence of this, a parameter reorganization method is usually used to solve this problem. The GPS L1/Galileo E1 SD-LC model with common-clock receiver is then represented by [33]:

$$\begin{aligned}
\Delta P_{kl,L1}^{i_G} &= \Delta\rho_{kl}^{i_G} + \alpha_{kl,L1}^{G} + \Delta\varepsilon_{kl,L1}^{i_G} \\
\Delta\varphi_{kl,L1}^{i_G} &= \Delta\rho_{kl}^{i_G} + \lambda_{L1}\cdot\left(\hat{\beta}_{kl,L1}^{G} + \Delta\nabla N_{kl,L1}^{1_G i_G}\right) + \Delta e_{kl,L1}^{i_G} \\
\Delta P_{kl,E1}^{j_E} &= \Delta\rho_{kl}^{j_E} + \alpha_{kl,E1}^{E} + \Delta\varepsilon_{kl,E1}^{j_E} \\
\Delta\varphi_{kl,E1}^{j_E} &= \Delta\rho_{kl}^{j_E} + \lambda_{E1}\cdot\left(\hat{\beta}_{kl,E1}^{E} + \Delta\nabla N_{kl,E1}^{1_E j_E}\right) + \Delta e_{kl,E1}^{j_E}
\end{aligned} \tag{2}$$

where $\hat{\beta}_{kl,L1}^{G} = \beta_{kl,L1}^{G} + N_{kl,L1}^{1_G}$ and $\hat{\beta}_{kl,E1}^{E} = \beta_{kl,E1}^{E} + N_{kl,E1}^{1_E}$ are the reorganized phase LBs, which are the sum of the original phase LB and the SD ambiguity of the reference satellite. They are reset when the reference satellite changes or a cycle slip occurs. $\Delta\nabla N_{kl,L1}^{1_G i_G} = \Delta N_{kl,L1}^{i_G} - \Delta N_{kl,L1}^{1_G}$ and $\Delta\nabla N_{kl,E1}^{1_E j_E} = \Delta N_{kl,E1}^{j_E} - \Delta N_{kl,E1}^{1_E}$ are the intra-system DD ambiguities between the non-reference satellite and the reference satellite of GPS and Galileo, respectively, where 1_G and 1_E are the reference satellites of GPS and Galileo, respectively. With Equation (2), the reorganized phase LBs can be estimated simultaneously with the baseline vector, the code LB, and the DD ambiguities.

2.2. SD-TC Model

From Equation (1) to Equation (2), the parameter reorganization is performed separately within each GNSS system. Fortunately, the code and phase LBs for GPS L1 and Galileo E1 are identical (i.e., $\alpha_{kl,L1}^{G} = \alpha_{kl,E1}^{E}$ and $\beta_{kl,L1}^{G} = \beta_{kl,E1}^{E}$) and the parameter reorganization can also be performed between GPS L1 and Galileo E1 SD observations. Assuming that 1_G is selected as the common reference satellite for the GPS and Galileo, the GPS L1/Galileo E1 SD-TC model is then represented by:

$$\begin{aligned}
\Delta P_{kl,L1}^{i_G} &= \Delta\rho_{kl}^{i_G} + \alpha_{kl,L1}^{G} + \Delta\varepsilon_{kl,L1}^{i_G} \\
\Delta\varphi_{kl,L1}^{i_G} &= \Delta\rho_{kl}^{i_G} + \lambda_{L1}\cdot\left(\hat{\beta}_{kl,L1}^{G} + \Delta\nabla N_{kl,L1}^{1_G i_G}\right) + \Delta e_{kl,L1}^{i_G} \\
\Delta P_{kl,E1}^{j_E} &= \Delta\rho_{kl}^{j_E} + \alpha_{kl,L1}^{G} + \Delta\varepsilon_{kl,E1}^{j_E} \\
\Delta\varphi_{kl,E1}^{j_E} &= \Delta\rho_{kl}^{j_E} + \lambda_{E1}\cdot\left(\hat{\beta}_{kl,L1}^{G} + \Delta\nabla N_{kl,L1E1}^{1_G j_E}\right) + \Delta e_{kl,E1}^{j_E}
\end{aligned} \tag{3}$$

where $\hat{\beta}^{G}_{kl,L1} = \beta^{G}_{kl,L1} + N^{1_G}_{kl,L1}$ is the reorganized phase LB, which is the sum of the original phase LB and the SD ambiguity of the reference satellite 1_G, and $\Delta\nabla N^{1_G j_E}_{kl,L1E1} = \Delta N^{j_E}_{kl,E1} - \Delta N^{1_G}_{kl,L1}$ is the inter-system DD ambiguity between the Galileo satellite and the GPS reference satellite 1_G. In the SD-TC model, the Galileo and GPS satellites are used as if they are from one constellation rather than two constellations. Compared with the SD-LC model, the SD-TC model takes advantage of the additional information that the code and phase LBs for GPS L1 and Galileo E1 are identical, and improved performance is therefore expected.

2.3. DD-LC Model

The troublesome code and phase LBs can be further eliminated by double-differencing. When a reference satellite is separately selected for GPS and Galileo, the GPS L1/Galileo E1 DD-LC model is represented by:

$$\begin{aligned}
\Delta\nabla P^{1_G i_G}_{kl,L1} &= \Delta\nabla\rho^{1_G i_G}_{kl} + \Delta\nabla\varepsilon^{1_G i_G}_{kl,L1} \\
\Delta\nabla\varphi^{1_G i_G}_{kl,L1} &= \Delta\nabla\rho^{1_G i_G}_{kl} + \lambda_{L1}\Delta\nabla N^{1_G i_G}_{kl,L1} + \Delta\nabla e^{1_G i_G}_{kl,L1} \\
\Delta\nabla P^{1_E j_E}_{kl,E1} &= \Delta\nabla\rho^{1_E j_E}_{kl} + \Delta\nabla\varepsilon^{1_E j_E}_{kl,E1} \\
\Delta\nabla\varphi^{1_E j_E}_{kl,E1} &= \Delta\nabla\rho^{1_E j_E}_{kl} + \lambda_{E1}\Delta\nabla N^{1_E j_E}_{kl,E1} + \Delta\nabla e^{1_E j_E}_{kl,E1}
\end{aligned} \tag{4}$$

where 1_G and 1_E are selected as the reference satellites of the GPS and Galileo, respectively. Only intra-system DD observations within each GNSS system are created when the DD-LC model is used.

2.4. DD-TC Model

For the common-clock receiver, the master and rover receivers are of the same type. The DISB between the GPS L1 and Galileo E1 is therefore close to zero and can be neglected. Consequently, the GPS and Galileo satellites can be treated as if they are from one constellation. Assuming that 1_G is selected as the common reference satellite for GPS and Galileo, the GPS L1/Galileo E1 DD-TC model with a common-clock receiver is then represented by [8,9,11]:

$$\begin{aligned}
\Delta\nabla P^{1_G i_G}_{kl,L1} &= \Delta\nabla\rho^{1_G i_G}_{kl} + \Delta\nabla\varepsilon^{1_G i_G}_{kl,L1} \\
\Delta\nabla\varphi^{1_G i_G}_{kl,L1} &= \Delta\nabla\rho^{1_G i_G}_{kl} + \lambda_{L1}\Delta\nabla N^{1_G i_G}_{kl,L1} + \Delta\nabla e^{1_G i_G}_{kl,L1} \\
\Delta\nabla P^{1_G j_E}_{kl,L1E1} &= \Delta\nabla\rho^{1_G j_E}_{kl} + \Delta\nabla\varepsilon^{1_G j_E}_{kl,L1E1} \\
\Delta\nabla\varphi^{1_G j_E}_{kl,L1E1} &= \Delta\nabla\rho^{1_G j_E}_{kl} + \lambda_{E1}\Delta\nabla N^{1_G j_E}_{kl,L1E1} + \Delta\nabla e^{1_G j_E}_{kl,L1E1}
\end{aligned} \tag{5}$$

Both the intra-system DD observations within the GPS and the inter-system DD observations between the GPS and Galileo are created when the DD-TC model is used. The model strength of the DD-TC model is stronger in comparison to the DD-LC model. As a result, improved performance is expected with the DD-TC model.

2.5. Comparison of the Four Models

The numbers of observation equations, estimates, and redundancies of the SD-LC, SD-TC, DD-LC, and DD-TC models in a single-epoch solution are listed in Table 1. In the single-epoch solution, compared with the DD-LC model, the DD-TC model introduces two additional observation equations and one additional DD ambiguity. Compared with the SD-LC model, the SD-TC model introduces one additional DD ambiguity but reduces two LB estimates. Therefore, compared to the loosely combined (DD-LC/SD-LC) model, one additional redundancy is introduced for the tightly combined (DD-TC/SD-TC) model, and the model strength is improved. Theoretically, the tightly combined (DD-TC/SD-TC) model is expected to provide improved performance with respect to the loosely combined (DD-LC/SD-LC) model. The advantages of the DD-TC model over the DD-LC model have been widely confirmed with empirical results in previous studies such as [8–14].

Moreover, compared with the DD-LC model, the SD-LC model introduces four additional observations as well as four LB estimates. Therefore, no redundancy is introduced,

and the model strength remains unchanged. Similarly, compared with the DD-TC model, the SD-TC model introduces two additional observation equations as well as two LB estimates, resulting in identical model strength for the two models. Therefore, identical results are theoretically expected for the SD model and the DD model. However, in the multi-epoch solution, the model strength of the SD model (SD-LC/SD-TC) can be improved if the phase and code LBs are modeled (e.g., time-constant or random walk model) and estimated over time, considering that the LBs are relatively stable in the time domain during a short time span within approximately one day [33]. In such a case, improved performance is expected for the SD model with respect to the DD model, and this has been confirmed both theoretically and empirically in previous studies such as [29,31–33].

Table 1. Comparison of the SD-LC, SD-TC, DD-LC, and DD-TC models in the single-epoch solution.

Model	SD-LC	SD-TC	DD-LC	DD-TC
Observation equation	$2n_G + 2n_E$	$2n_G + 2n_E$	$2n_G + 2n_E - 4$	$2n_G + 2n_E - 2$
Position parameter	3	3	3	3
DD ambiguity	$n_G + n_E - 2$	$n_G + n_E - 1$	$n_G + n_E - 2$	$n_G + n_E - 1$
LB parameter	4	2	none	none
Observation redundancy	$n_G + n_E - 5$	$n_G + n_E - 4$	$n_G + n_E - 5$	$n_G + n_E - 4$

3. Experimental Data

Static short-baseline data collected with a Trimble BD992 dual-antenna common-clock receiver and two TRM59900.00 NONE antennas at the campus of Wuhan University were used in this research. Detailed information about the experimental data is listed in Table 2. The involved GNSS equipment and the observational environment are shown in Figure 1. It is worth noting that two coaxial cables with the same material and length were used to connect the two antennas and the receiver. Figure 2 shows the numbers of observed GPS/Galileo satellites as well as the position dilution of precision (PDOP) series of combined GPS/Galileo under a 10° elevation cutoff angle. The observed GPS, Galileo, and GPS/Galileo satellites during the entire time span were 6–11, 5–9, and 11–19, respectively. The average numbers of visible satellites were 8.7, 6.3, and 15.0, respectively. The GPS/Galileo PDOP was about 1.14–2.00, with an average of about 1.41.

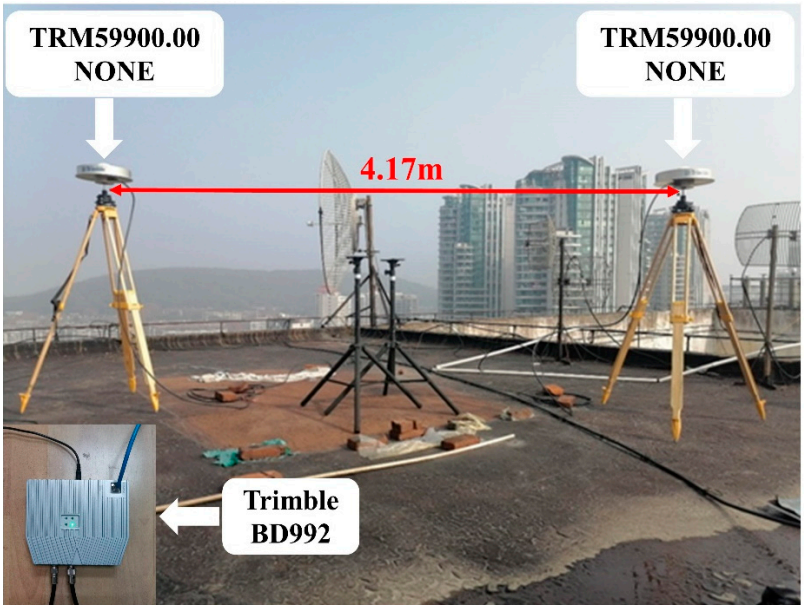

Figure 1. Observational equipment and condition.

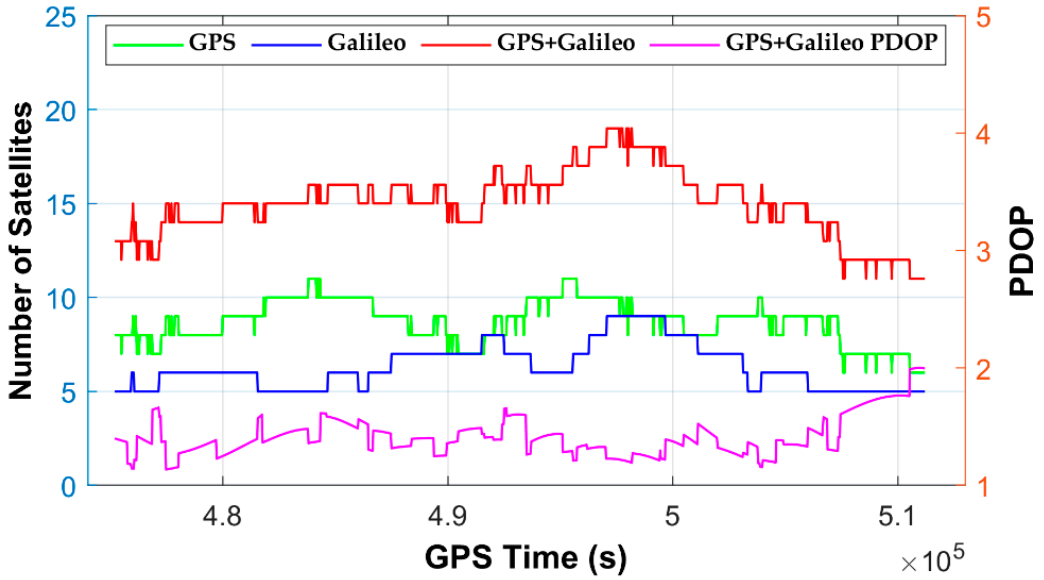

Figure 2. Numbers of GPS/Galileo satellites and the PDOP series of combined GPS/Galileo under a 10° elevation cutoff angle.

Table 2. Detailed information about the experimental data.

Option	Experimental Information
Site	On the roof of a high-rise building, Wuhan University
Time	From approximately 12:00 to 22:00 on 17 January 2020, GPS time
Sampling interval	30 s
GNSS receiver	Trimble BD992
GNSS antenna	TRM59900.00 NONE
Cable	Two identical coaxial cables
Baseline length	About 4.17 m

4. Results and Validation

4.1. Data Processing Strategy

In this article, the GPS L1/Galileo E1 attitude determination performances of the DD-LC, DD-TC, SD-LC, and SD-TC models were evaluated and compared in both the single-epoch and multi-epoch modes. The performances of the four models were evaluated in aspects of the ADOP, the AR success and failure rates, and the positioning and attitude accuracy.

In the data processing procedure, the widely used elevation-dependent function in [38] was used in the stochastic model, and the model coefficients were set to 3 mm and 0.3 m for the phase and code, respectively. In the single-epoch solution, the baseline coordinates, the ambiguities, and the code and phase LBs in the SD-LC and SD-TC models were estimated epoch-wise. In the multi-epoch solution, however, the ambiguities and the code and phase LBs in the SD-LC and SD-TC models were estimated with a random walk model with a relatively low process noise, considering that they were stable in the time domain. The corresponding process noise values were 1×10^{-6} m/sqrt(s), 1×10^{-4} m/sqrt(s), and 1×10^{-6} m/sqrt(s), respectively. After the float solution was obtained, the ambiguities were fixed using the least-squares ambiguity decorrelation adjustment (LAMBDA) method [39], and the widely used ratio test [40] with an empirical threshold of 3.0 was adopted to validate the ambiguities. For our dual-antenna GNSS-based attitude determination system, the yaw and pitch were computed using the direct computation method [41] by using the baseline vector of the slave antenna with respect to the master antenna in the local-level system. Additionally, different elevation cutoff angles

(10°, 20°, 30°, 40°, and 45°) were set to simulate different observational conditions and satellite visibilities.

The empirical AR success rate is defined as the percentage of accepted and correctly fixed epochs compared to the total number of epochs in the entire time span. The empirical AR failure rate was defined as the percentage of accepted and incorrectly fixed epochs compared to the total number of epochs [42]. The fixed ambiguities were accepted when the ratio test was passed. Whether they were further considered to be correctly fixed or incorrectly fixed depended on whether the baseline error in the east (E)/north (N)/up (U) was less than 2 cm/2 cm/4 cm. The reference true baseline vector was the GPS/Galileo L1/E1 static fixed solution. The true attitude was computed using the reference true baseline vector.

4.2. Performance Comparison of the Single-Epoch Solutions

4.2.1. ADOP

As a representative example, Figure 3 shows the ADOP series of the DD-LC, DD-TC, SD-LC, and SD-TC models under a 40° elevation cutoff angle in the single-epoch solution. Since the epoch-by-epoch ADOP values of the DD-LC and DD-TC models were identical to those of the SD-LC and SD-TC models, respectively, the ADOP series of the DD-LC and DD-TC models are not visible in the figure. This is in line with the theoretical analysis in Section 2. The mean ADOP values of the DD-LC, DD-TC, SD-LC, and SD-TC models during the entire time span under different elevation cutoff angles are listed in Table 3. As expected, the mean ADOP values of the DD-LC and SD-LC models were identical, and the same was true for the DD-TC and SD-TC models. Moreover, the ADOP values of the tightly combined models (DD-TC and SD-TC) were much lower than those of the loosely combined models (DD-LC and SD-LC), especially in the case of a high elevation cutoff angle. The mean ADOP values were decreased from 0.180, 0.211, 0.331, and 1.145 to 0.152, 0.170, 0.237, and 0.525 cycles, respectively. Theoretically, the ambiguity resolution performances of the tightly combined models were expected to be superior to the loosely combined models.

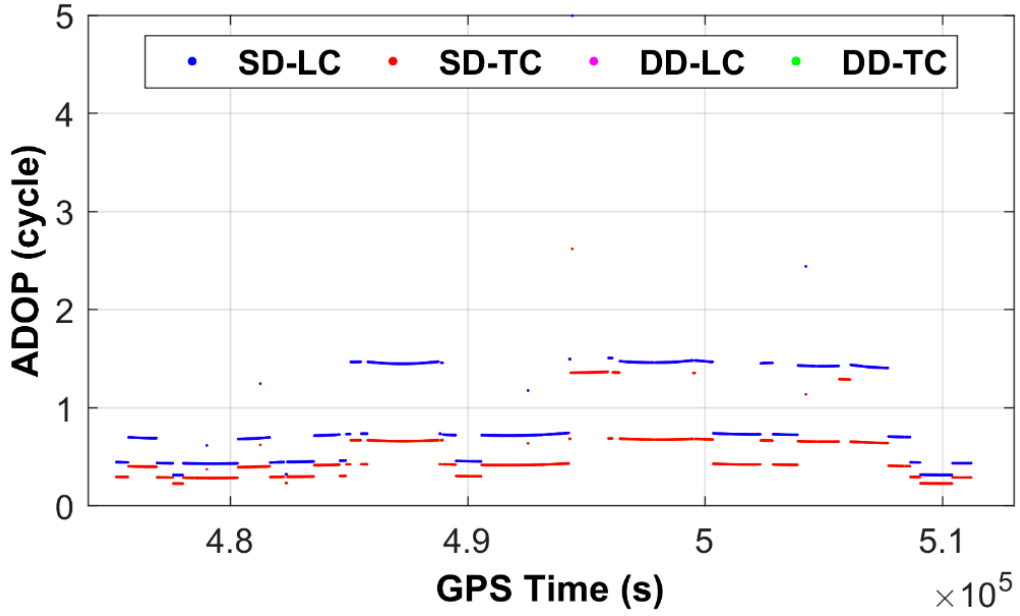

Figure 3. ADOP series of the DD-LC, DD-TC, SD-LC, and SD-TC models under a 40° elevation cutoff angle in the single-epoch solution.

Table 3. The mean ADOP values of the DD-LC, DD-TC, SD-LC, and SD-TC models under different elevation cutoff angles in the single-epoch solution.

Elevation Cutoff Angle	DD-LC/SD-LC (Cycle)	DD-TC/SD-TC (Cycle)
10°	0.180	0.152
20°	0.211	0.170
30°	0.331	0.237
40°	1.145	0.525

4.2.2. AR Success and Failure Rates

Table 4 lists the AR success and failure rates under different elevation cutoff angles in the single-epoch solution. It was observed that the AR success and failure rates of the DD-LC and SD-LC models were identical, and the same was true for the DD-TC and SD-TC models. Moreover, we found that compared with the loosely combined models (DD-LC and SD-LC), the tightly combined models (DD-TC and SD-TC) provided a much larger AR success rate and a lower failure rate above a 10° elevation cutoff angle. The AR success rates of the loosely combined models were increased from approximately 99.7%, 89.5%, and 30.0% to 99.9%, 98.1%, and 65.1% by approximately 0.2%, 8.6%, and 35.1% under 20°, 30°, and 40° elevation cutoff angles, respectively. The AR failure rate was decreased from 6.1% to 1.8% by approximately 4.3% under a 40° elevation cutoff angle.

Table 4. The AR success and failure rates of the DD-LC, DD-TC, SD-LC, and SD-TC models under different elevation cutoff angles in the single-epoch solution.

Elevation Cutoff Angle	AR Success Rate (Percent)		AR Failure Rate (Percent)	
	DD-LC/SD-LC	DD-TC/SD-TC	DD-LC/SD-LC	DD-TC/SD-TC
10°	99.9	99.9	0	0
20°	99.7	99.9	0	0
30°	89.5	98.1	0	0
40°	30.0	65.1	6.1	1.8

4.2.3. Positioning Accuracy

Figure 4 shows the three-dimensional positioning error series of the correctly fixed solutions for the four models under different elevation cutoff angles in the single-epoch solution. The corresponding root-mean-square (RMS) errors are listed in Table 5. Similarly, the epoch-by-epoch three-dimensional positioning errors of the DD-LC and DD-TC models were identical to those of the SD-LC and SD-TC models, respectively. Therefore, the positioning errors of the DD-LC and DD-TC models are not visible in the figure, and the positioning RMS errors of the DD-LC and DD-TC models are identical to the SD-LC and SD-TC models, respectively. Moreover, the positioning RMS errors of the tightly combined models were comparable to those of the loosely combined models. Additionally, the positioning RMS errors increased significantly with an increase in the elevation cutoff angle.

Table 5. The positioning RMS errors of the DD-LC, DD-TC, SD-LC, and SD-TC models under different elevation cutoff angles in the single-epoch solution.

Elevation Cutoff Angle	E (cm)		N (cm)		U (cm)	
	DD-LC/SD-LC	DD-TC/SD-TC	DD-LC/SD-LC	DD-TC/SD-TC	DD-LC/SD-LC	DD-TC/SD-TC
10°	0.15	0.14	0.17	0.17	0.44	0.42
20°	0.16	0.15	0.18	0.18	0.50	0.48
30°	0.18	0.18	0.20	0.20	0.76	0.68
40°	0.23	0.25	0.25	0.29	1.12	1.10

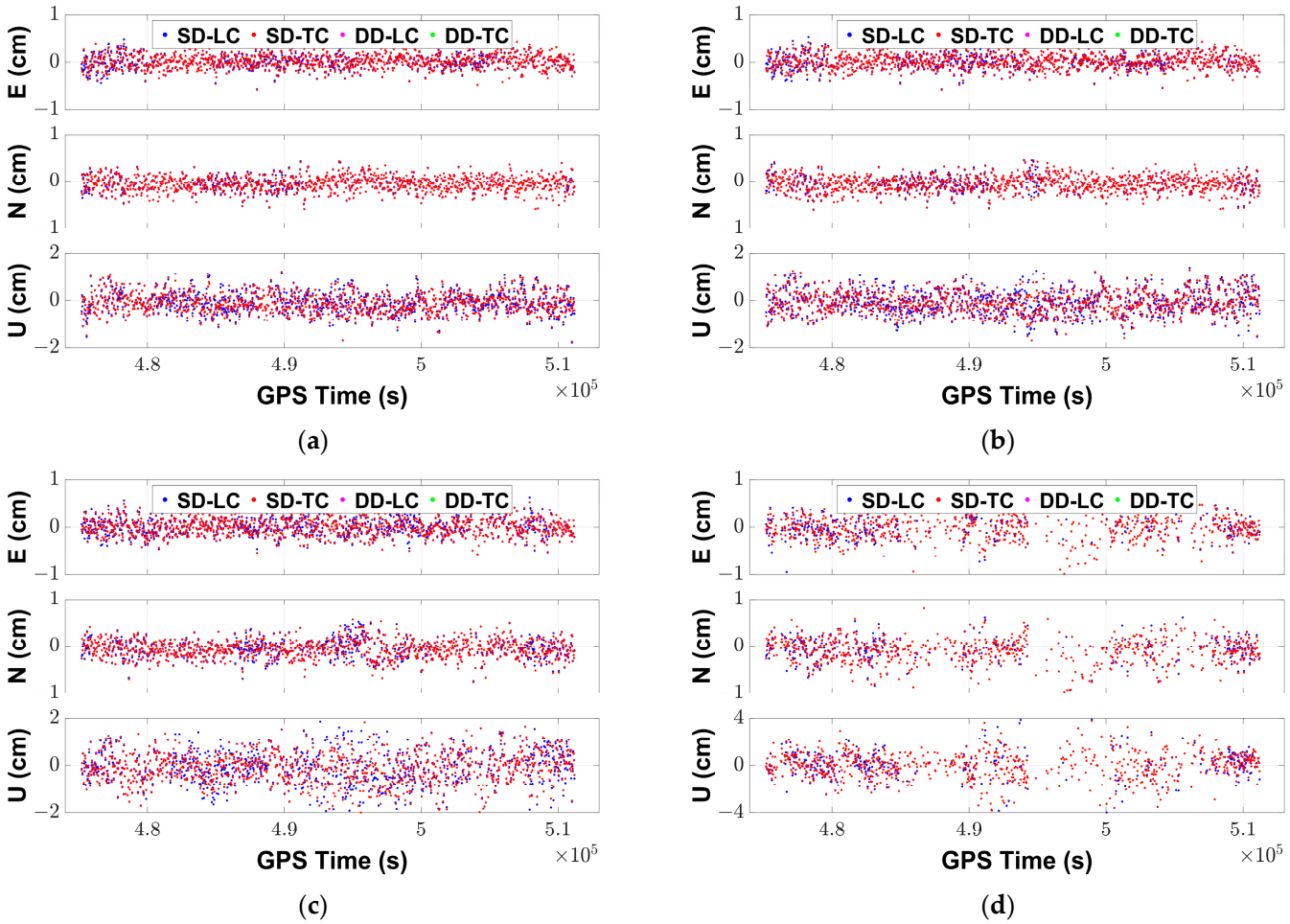

Figure 4. The positioning error series of the DD-LC, DD-TC, SD-LC, and SD-TC models under different elevation cutoff angles in the single-epoch solution: (**a**) 10°; (**b**) 20°; (**c**) 30°; and (**d**) 40°.

4.2.4. Attitude Accuracy

Figure 5 shows the attitude (yaw and pitch) error series of the correctly fixed solutions for the four models under different elevation cutoff angles in the single-epoch solution. The corresponding RMS errors for a baseline separation of 1 m are listed in Table 6. Similarly, the attitude RMS errors of the DD-LC and DD-TC models were identical to those of SD-LC and SD-TC models, respectively. Moreover, the attitude RMS errors of the tightly combined models were comparable to those of the loosely combined models. The RMS errors increased significantly with an increase in the elevation cutoff angle.

Table 6. The yaw and pitch RMS errors of the DD-LC, DD-TC, SD-LC, and SD-TC models under different elevation cutoff angles in the single-epoch solution.

Elevation Cutoff Angle	Yaw (°)		Pitch (°)	
	DD-LC/SD-LC	DD-TC/SD-TC	DD-LC/SD-LC	DD-TC/SD-TC
10°	0.09	0.09	0.25	0.24
20°	0.09	0.09	0.29	0.28
30°	0.11	0.11	0.44	0.39
40°	0.13	0.16	0.64	0.63

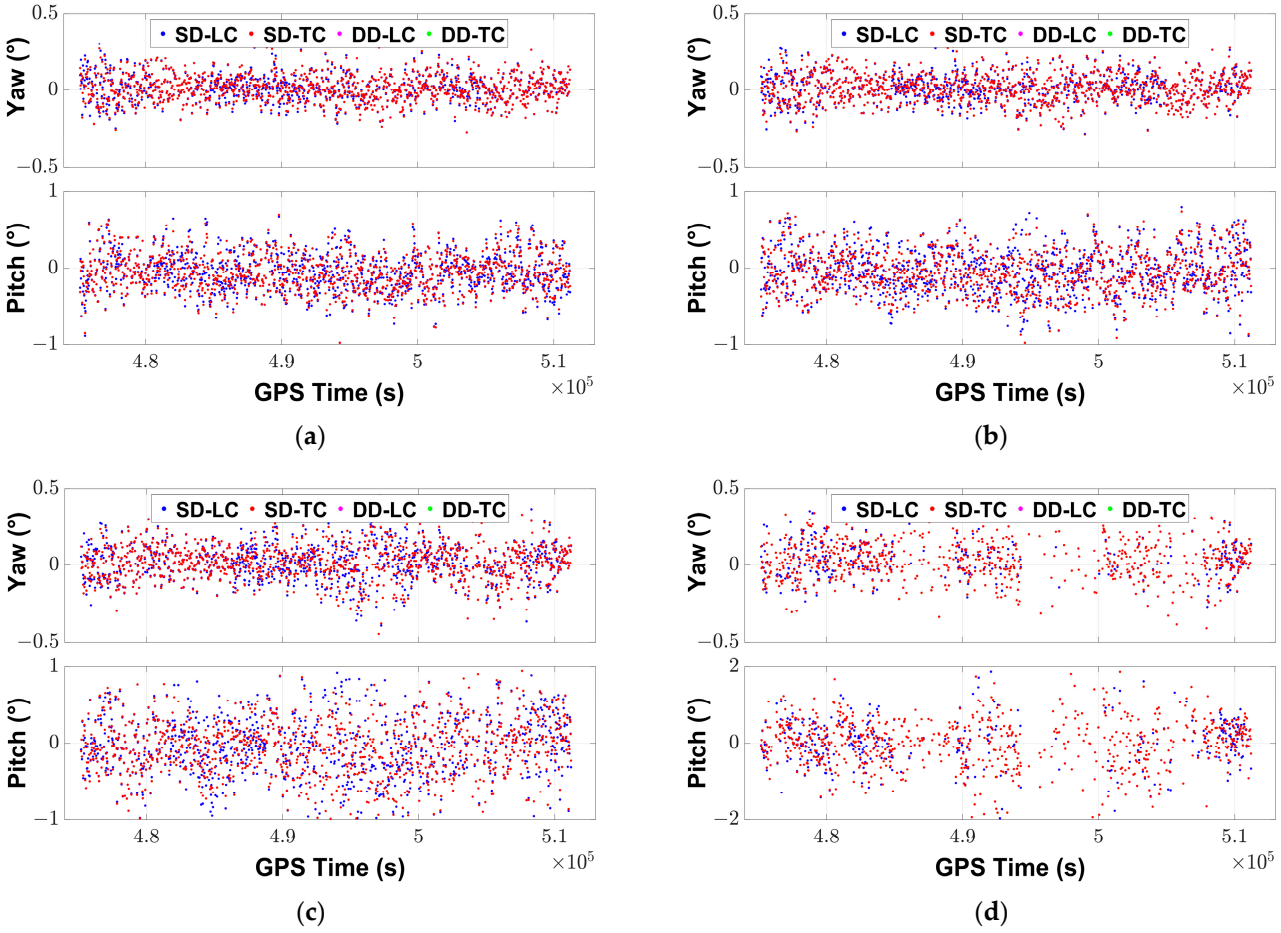

Figure 5. The yaw and pitch error series of the DD-LC, DD-TC, SD-LC, and SD-TC models under different elevation cutoff angles in the single-epoch solution: (**a**) 10°; (**b**) 20°; (**c**) 30°; and (**d**) 40°.

4.3. Performance Comparison of the Multi-Epoch Solutions

4.3.1. ADOP

As a representative example, Figure 6 shows the ADOP series of the DD-LC, DD-TC, SD-LC, and SD-TC models under a 45° elevation cutoff angle in the multi-epoch solution. The mean ADOP values of the four models during the entire time span under different elevation cutoff angles are listed in Table 7. It was observed that the ADOP values of the DD-TC model were lower than those of the DD-LC model, especially in the case of a high elevation cutoff angle. For example, the mean ADOP values under 40° and 45° elevation cutoff angles were 0.017 and 0.041 cycles for DD-LC model and were decreased to 0.010 and 0.015 cycles for DD-TC model, respectively. Although the mean ADOP values of the SD-TC model were lower than those of the DD-LC model, it is, however, worth noting that the epoch-by-epoch ADOP value of SD-TC model was not always smaller than that of the SD-LC model (as shown in Figure 6). This is reasonable, considering that the ADOP computed with these two models could be influenced by the process noise of the ambiguity and LB parameters. Moreover, whether for the loosely or tightly combined models, the ADOP values of the SD models (SD-LC and SD-TC) were much lower than those of the DD models (DD-LC and DD-TC). For example, the mean ADOP values for the 10°, 20°, 30°, 40°, and 45° elevation cutoff angles were 0.008, 0.008, 0.010, 0.017, and 0.041 cycles for the DD-LC model and were decreased to 0.007, 0.007, 0.008, 0.010, and 0.015 cycles for the SD-LC model.

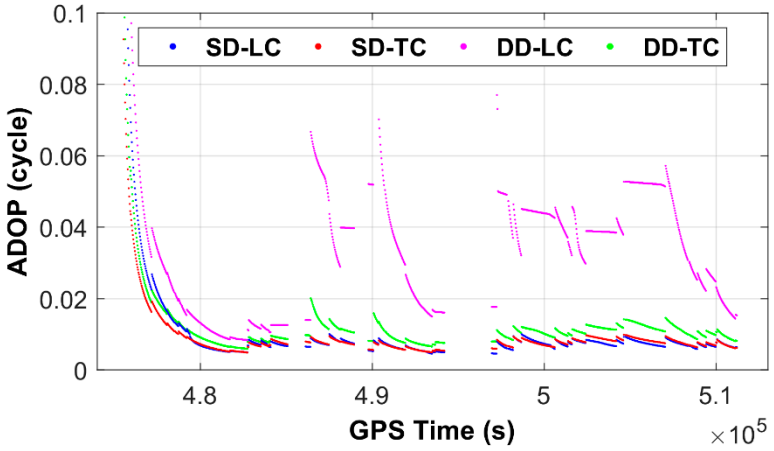

Figure 6. The ADOP series of the DD-LC, DD-TC, SD-LC, and SD-TC models under a 45° elevation cutoff angle in the multi-epoch solution.

Table 7. The mean ADOP values of the DD-LC, DD-TC, SD-LC, and SD-TC models under different elevation cutoff angles in the multi-epoch solution.

Elevation Cutoff Angle	DD-LC (Cycle)	DD-TC (Cycle)	SD-LC (Cycle)	SD-TC (Cycle)
10°	0.008	0.007	0.007	0.006
20°	0.008	0.007	0.007	0.006
30°	0.010	0.008	0.008	0.007
40°	0.017	0.010	0.010	0.009
45°	0.041	0.015	0.015	0.012

4.3.2. AR Success and Failure Rates

Table 8 lists the AR success and failure rates of the DD-LC, DD-TC, SD-LC, and SD-TC models under different elevation cutoff angles in the multi-epoch solution. It was found that the AR success rates of the four models were all 100% under 10°, 20°, and 30° elevation cutoff angles. However, in case of 40° and 45° elevation cutoff angles, the advantages of the tightly combined model over the loosely combined model as well as the SD model over the DD model were exhibited. For both the SD and DD models, the tightly combined model delivered a much higher AR success rate and a lower AR failure rate with respect to the loosely combined model. For example, the AR success rates under a 45° elevation cutoff angle were improved from approximately 74.8% and 98.8% for the DD-LC and SD-LC models to approximately 91.5% and 99.4% for the DD-TC and SD-TC models, by approximately 16.7% and 0.6%, respectively. The AR failure rates were reduced from approximately 20.8% and 0.9% for the DD-LC and SD-LC models to 8.4% and 0.6% for the DD-TC and SD-TC models, by approximately 12.4% and 0.3%, respectively. Moreover, for both the loosely combined and tightly combined models, the SD model improved the AR success rate and reduced the AR failure rate with respect to the DD model. Compared with the DD-LC and DD-TC models, the AR success rates of the SD-LC and SD-TC models were improved by approximately 24.0% and 7.9%, respectively, and the AR failure rates were reduced by approximately 19.9% and 7.8%, respectively.

Table 8. The AR success and failure rates of the DD-LC, DD-TC, SD-LC, and SD-TC models under different elevation cutoff angles in the multi-epoch solution.

Elevation Cutoff Angle	AR Success Rate (Percent)				AR Failure Rate (Percent)			
	DD-LC	DD-TC	SD-LC	SD-TC	DD-LC	DD-TC	SD-LC	SD-TC
10°	100	100	100	100	0	0	0	0
20°	100	100	100	100	0	0	0	0
30°	100	100	100	100	0	0	0	0
40°	92.5	97.5	100	100	7.5	2.5	0	0
45°	74.8	91.5	98.8	99.4	20.8	8.4	0.9	0.6

4.3.3. Positioning Accuracy

Figure 7 shows the three-dimensional positioning error series of the correctly fixed solutions for the DD-LC, DD-TC, SD-LC, and SD-TC models under different elevation cutoff angles in the multi-epoch solution, and the corresponding RMS errors are listed in Table 9. Similar to the single-epoch results, the positioning RMS errors of the tightly combined models were comparable to those of the loosely combined models, and the positioning RMS errors increased with an increase in the elevation cutoff angle. However, different from the single-epoch results, for both the loosely combined and tightly combined models, the SD model provided comparable positioning RMS error in the east and north components and significantly lower RMS error in the vertical component with respect to the DD model. Compared with the DD-LC model, the positioning RMS errors in the vertical component of the SD-LC model were reduced from approximately 0.42, 0.52, 0.84, 1.43, and 1.66 cm to 0.13, 0.14, 0.22, 0.39, and 0.54 cm, by approximately 69.0%, 73.1%, 73.8%, 72.7%, and 67.5%, under 10°, 20°, 30°, 40°, and 45° elevation cutoff angles, respectively. Similarly, compared with the DD-TC model, the positioning RMS errors in the vertical component of the SD-TC model were reduced by approximately 65.0%, 69.4%, 74.3%, 71.5%, and 68.6%, respectively.

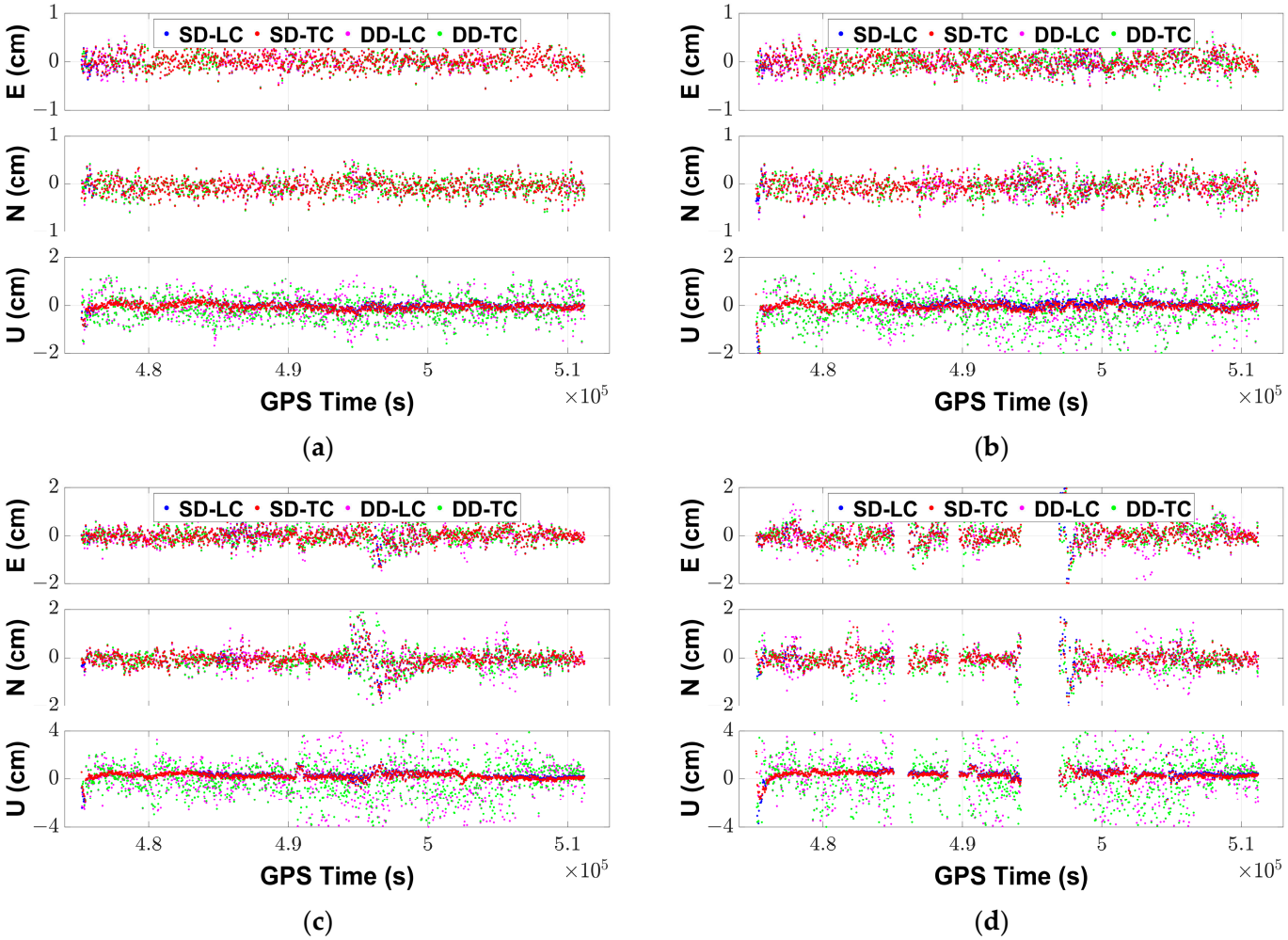

Figure 7. The positioning error series of the DD-LC, DD-TC, SD-LC, and SD-TC models under different elevation cutoff angles in the multi-epoch solution: (**a**) 20°; (**b**) 30°; (**c**) 40°; and (**d**) 45°.

Table 9. The positioning RMS errors of the DD-LC, DD-TC, SD-LC, and SD-TC models under different elevation cutoff angles in the multi-epoch solution.

Elevation Cutoff Angle	E (cm)				N (cm)				U (cm)			
	DD-LC	DD-TC	SD-LC	SD-TC	DD-LC	DD-TC	SD-LC	SD-TC	DD-LC	DD-TC	SD-LC	SD-TC
10°	0.15	0.14	0.14	0.14	0.17	0.16	0.16	0.16	0.42	0.40	0.13	0.14
20°	0.15	0.15	0.15	0.15	0.18	0.18	0.17	0.17	0.52	0.49	0.14	0.15
30°	0.18	0.18	0.17	0.17	0.21	0.21	0.19	0.19	0.84	0.70	0.22	0.18
40°	0.32	0.29	0.27	0.27	0.42	0.38	0.32	0.32	1.43	1.23	0.39	0.35
45°	0.42	0.39	0.34	0.34	0.44	0.41	0.33	0.33	1.66	1.56	0.54	0.49

4.3.4. Attitude Accuracy

Figure 8 shows the attitude (yaw and pitch) error series of the correctly fixed solutions for the DD-LC, DD-TC, SD-LC, and SD-TC models under different elevation cutoff angles in the multi-epoch solution, and the corresponding RMS errors for a baseline separation of 1 m are listed in Table 10. Similar to the positioning accuracy results, we observed that for both the SD and DD models the attitude RMS errors of the tightly combined models were comparable to those of the loosely combined models. Moreover, for both the loosely combined and tightly combined models, compared with the DD model, the SD model delivered comparable RMS error for yaw but significantly lower RMS error for pitch. Compared with the DD-LC model, the pitch RMS error for the SD-LC model under 10°, 20°, 30°, 40°, and 45° elevation cutoff angles was reduced from approximately 0.24°, 0.30°, 0.48°, 0.82°, and 0.95° to approximately 0.08°, 0.08°, 0.12°, 0.22°, and 0.31°, by approximately 66.7%, 73.3%, 75.0%, 73.2%, and 67.4%, respectively. Similarly, compared with the DD-TC model, the improvements in pitch accuracy for the SD-TC model were approximately 65.2%, 67.9%, 72.5%, 71.4%, and 68.5%, respectively.

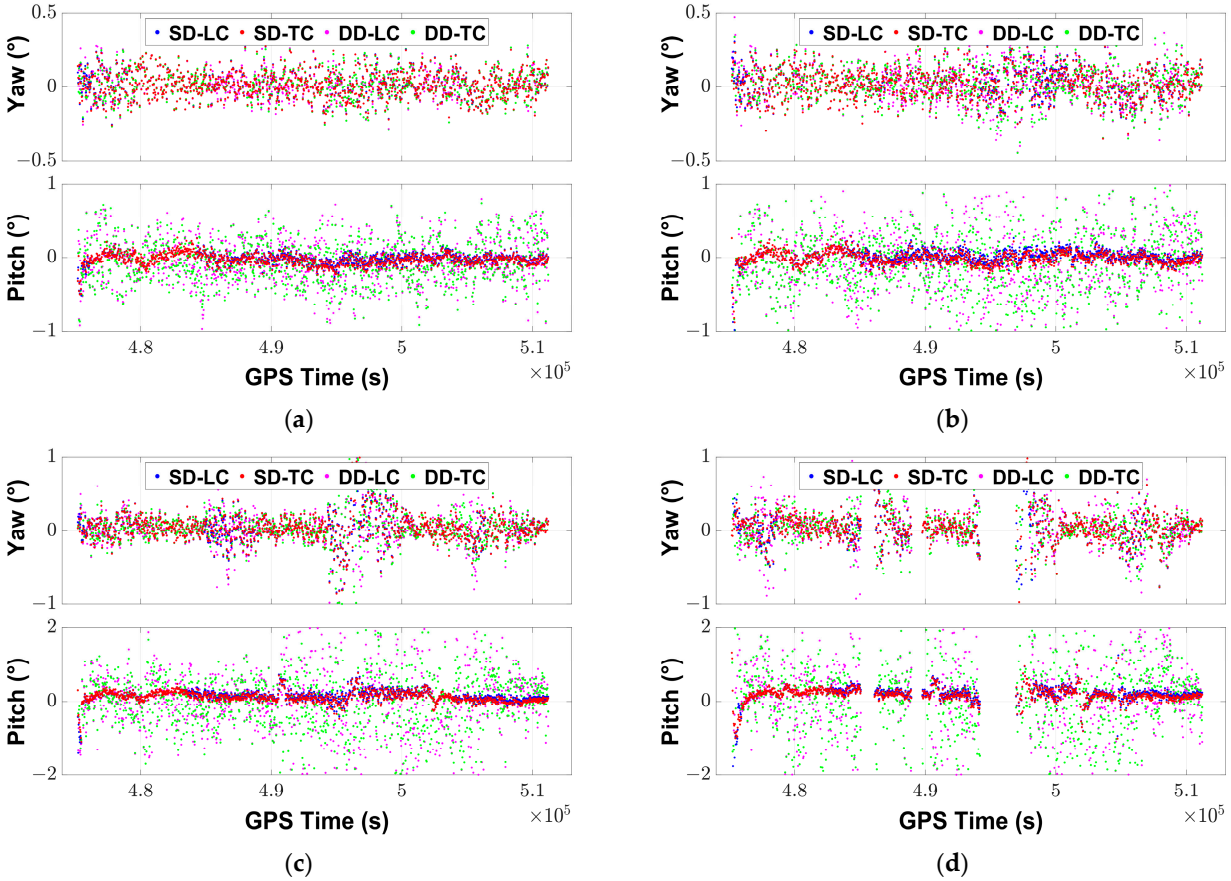

Figure 8. The yaw and pitch error series of the DD-LC, DD-TC, SD-LC, and SD-TC models under different elevation cutoff angles in the multi-epoch solution: (**a**) 20°; (**b**) 30°; (**c**) 40°; and (**d**) 45°.

Table 10. The yaw and pitch RMS errors of the DD-LC, DD-TC, SD-LC, and SD-TC models under different elevation cutoff angles in the multi-epoch solution.

Elevation Cutoff Angle	Yaw (°)				Pitch (°)			
	DD-LC	DD-TC	SD-LC	SD-TC	DD-LC	DD-TC	SD-LC	SD-TC
10°	0.09	0.09	0.08	0.08	0.24	0.23	0.08	0.08
20°	0.09	0.09	0.09	0.09	0.30	0.28	0.08	0.09
30°	0.12	0.12	0.10	0.10	0.48	0.40	0.12	0.11
40°	0.24	0.22	0.20	0.20	0.82	0.70	0.22	0.20
45°	0.25	0.25	0.23	0.23	0.95	0.89	0.31	0.28

5. Discussion

For the dedicated common-clock receiver, the master and rover receivers share the same clock and are of the same type, which offers the possibility for GNSS-based attitude determination with the SD model as well as the tightly combined DD model. In this contribution, for the first time, we present model and performance comparisons of GPS L1/Galileo E1 attitude determination with a common-clock receiver using the SD-LC, SD-TC, DD-LC, and DD-TC models. Our experimental results and main findings are in agreement with previous studies and further show the potential of high-precision multi-GNSS attitude determination with a common-clock receiver. With regard to the comparison of the loosely and tightly combined models, our experimental results revealed that the DD-TC model outperformed the DD-LC model for both the single-epoch and multi-epoch solutions, which has been reported in previous studies [8–16]. Furthermore, the advantage of the SD-TC model over the SD-LC model is presented. With regard to the comparison of the SD and DD models, we found that in the single-epoch mode the results of the SD models were identical to those of the DD models, i.e., the results of the SD-LC and SD-TC models were identical to the DD-LC and DD-TC models, respectively. These numerical results further confirm the theoretical analyses in the previous studies [28,29]. Moreover, we confirm the advantage of the SD model over the DD model in the multi-epoch mode, as demonstrated in the literature [29–33,37], and further show the benefits of the SD-TC model over the DD-TC model.

It is noted that, while our research is based on GPS L1/Galileo E1 observations, the methodology can be extended to the multi-GNSS multi-frequency case (e.g., GPS L1-L5/Galileo E1-E5a/BDS-3 B1C-B2a) as well. Moreover, only static data were processed with simulated observational conditions and satellite visibilities in this research. More static and kinematic datasets will therefore be tested to further compare the performances of the four models and validate our results in the future. In-depth investigation on the comparison of the four models with a theoretical derivation of the mathematical model is also required.

6. Conclusions

In this contribution, for the first time, we focused on evaluating the performance of GPS L1/Galileo E1 precise relative positioning and attitude determination with the SD-LC, SD-TC, DD-LC, and DD-TC models based on a common-clock receiver in both single-epoch and multi-epoch modes. The performances of the four models were evaluated in terms of the ADOP, the AR success and failure rates, and the positioning and attitude accuracy using static short-baseline data collected with a Trimble BD992 dual-antenna common-clock receiver. The following conclusions can be drawn:

(1) For both the single-epoch and multi-epoch solutions, the experimental results confirmed the advantages of the tightly combined model over the loosely combined model. Compared with the loosely combined models (SD-LC/DD-LC), the tightly combined models (SD-TC/DD-TC) provided higher AR success rates and lower AR failure rates, especially under high elevation cutoff angles. Meanwhile, their three-dimensional positioning and attitude accuracy were comparable. In the case of the

single-epoch solution, the AR success rates were increased from approximately 99.7%, 89.5%, and 30.0% for the DD-LC and SD-LC models to 99.9%, 98.1%, and 65.1% for the DD-TC and SD-TC models, by approximately 0.2%, 8.6%, and 35.1%, under 20°, 30°, and 40° elevation cutoff angles, respectively. The AR failure rate was decreased from 6.1% to 1.8%, by approximately 4.3%, under a 40° elevation cutoff angle. In the case of the multi-epoch solution, the AR success rates were improved from approximately 74.8% and 98.8% to approximately 91.5% and 99.4%, by approximately 16.7% and 0.6%, under a 45° elevation cutoff angle, respectively. The AR failure rates were reduced from approximately 20.8% and 0.9% to 8.4% and 0.6%, by approximately 12.4% and 0.3%, respectively.

(2) For the single-epoch solution, the experimental results revealed that the results of the SD models were identical to those of the DD models, i.e., the results of the SD-LC and SD-TC models were identical to those of DD-LC and DD-TC models, respectively. For the multi-epoch solution, however, the experimental results confirmed the advantage of the SD model over the DD model. Compared with the DD model, the SD model provided a smaller ADOP value, a higher AR success rate, and a lower failure rate, especially under a high elevation cutoff angle. In the case of a 45° elevation cutoff angle, compared with the DD-LC and DD-TC models, the AR success rates of the SD-LC and SD-TC models were improved by approximately 24.0% and 7.9%, respectively, and the AR failure rates were reduced by approximately 19.9% and 7.8%, respectively. Meanwhile, compared with the DD model, the SD model delivered comparable positioning accuracy in the horizontal component (and yaw accuracy) and substantially better accuracy in the vertical component (and pitch accuracy) under different elevation cutoff angles. The positioning RMS error in the vertical component was reduced by approximately 65.0–74.3%. The pitch accuracy was improved by approximately 65.2–75.0%.

Author Contributions: Conceptualization, M.W. and W.L.; methodology, M.W., J.L. and S.L.; software, M.W., J.L. and S.L.; validation, J.L. and M.W.; formal analysis, M.W. and J.L.; writing—original draft preparation, J.L., W.L. and M.W.; writing—review and editing, M.W. and W.L. All authors have read and agreed to the published version of the manuscript.

Funding: This research was funded by the Hubei Provincial Natural Science Foundation of China, grant number 2019CFB261; the National Natural Science Foundation of China, grant numbers 41904035 and 41774031; the Key Laboratory for Digital Land and Resources of Jiangxi Province, East China University of Technology, grant number DLLJ202106; and the Key Laboratory of Geospace Environment and Geodesy, Ministry of Education, Wuhan University, grant number 19-01-06.

Data Availability Statement: The raw GNSS observations are not publicly available. For more details, please contact the corresponding author by email: wkliu@sgg.whu.edu.cn.

Acknowledgments: The authors appreciate the constructive and valuable comments from the anonymous reviewers.

Conflicts of Interest: The authors declare no conflict of interest.

Abbreviations

The following abbreviations are used in this manuscript:

ADOP	ambiguity dilution of precision
AR	ambiguity resolution
BDS-3	BeiDou global navigation satellite system
DD	double-differenced
DD-LC	loosely combined double-differenced
DD-TC	tightly combined double-differenced
DISB	differential inter-system bias
Galileo	Galileo navigation satellite system
GNSS	global navigation satellite system

GPS	global positioning system
INS	inertial navigation system
IRNSS	Indian Regional Navigation Satellite System
LAMBDA	least-squares ambiguity decorrelation adjustment
LB	line bias
PDOP	position dilution of precision
QZSS	Quasi-Zenith Satellite System
RMS	root mean square
SD	single-differenced
SD-LC	loosely combined single-differenced
SD-TC	tightly combined single-differenced

References

1. Wang, Y.; Zhan, X.; Zhang, Y. Improved ambiguity function method based on analytical resolution for GPS attitude determination. *Meas. Sci. Technol.* **2007**, *18*, 2985–2990. [CrossRef]
2. Zhu, F.; Hu, Z.; Liu, W.; Zhang, X. Dual-Antenna GNSS Integrated with MEMS for Reliable and Continuous Attitude Determination in Challenged Environments. *IEEE Sens. J.* **2019**, *19*, 3449–3461. [CrossRef]
3. Zhang, P.; Zhao, Y.; Lin, H.; Zou, J.; Wang, X.; Yang, F. A Novel GNSS Attitude Determination Method Based on Primary Baseline Switching for A Multi-Antenna Platform. *Remote Sens.* **2020**, *12*, 747. [CrossRef]
4. Zhang, X.; Wu, M.; Liu, W. Receiver time misalignment correction for GPS-based attitude determination. *J. Navig.* **2015**, *68*, 646–664. [CrossRef]
5. Wu, S.; Zhao, X.; Pang, C.; Zhang, L.; Xu, Z.; Zou, K. Improving ambiguity resolution success rate in the joint solution of GNSS-based attitude determination and relative positioning with multivariate constraints. *GPS Solut.* **2020**, *24*, 1–14. [CrossRef]
6. Willi, D.; Rothacher, M. GNSS attitude determination with non-synchronized receivers and short baselines onboard a spacecraft. *GPS Solut.* **2017**, *21*, 1605–1617. [CrossRef]
7. Wang, X.; Yao, Y.; Xu, C.; Zhao, Y.; Lv, D. An Improved Single-Epoch Attitude Determination Method for Low-Cost Single-Frequency GNSS Receivers. *Remote Sens.* **2021**, *13*, 2746. [CrossRef]
8. Wu, M.; Zhang, X.; Liu, W.; Ni, S.; Yu, S. Tightly combined BeiDou B2 and Galileo E5b signals for precise relative positioning. *J. Navig.* **2017**, *70*, 1253–1266. [CrossRef]
9. Wu, M.; Zhang, X.; Liu, W.; Wu, R.; Zhang, R.; Le, Y.; Wu, Y. Influencing factors of differential inter-system bias and performance assessment of tightly combined GPS, Galileo, and QZSS relative positioning for short baseline. *J. Navig.* **2019**, *72*, 965–986. [CrossRef]
10. Li, W.; Zhu, S.; Ming, Z. Estimation of Inter-System Biases between BDS-3/GPS/Galileo and Its Application in RTK Positioning. *Remote Sens.* **2021**, *13*, 3507. [CrossRef]
11. Wu, M.; Liu, W.; Wang, W.; Zhang, X. Differential Inter-System Biases Estimation and Initial Assessment of Instantaneous Tightly Combined RTK with BDS-3, GPS, and Galileo. *Remote Sens.* **2019**, *11*, 1430. [CrossRef]
12. Odijk, D.; Nadarajah, N.; Zaminpardazm, S.; Teunissen, P.J.G. GPS, Galileo, QZSS and IRNSS differential ISBs: Estimation and application. *GPS Solut.* **2016**, *21*, 439–450. [CrossRef]
13. Odijk, D.; Teunissen, P.J.G. Characterization of between receiver GPS-Galileo inter-system biases and their effect on mixed ambiguity resolution. *GPS Solut.* **2013**, *17*, 521–533. [CrossRef]
14. Paziewski, J.; Wielgosz, P. Accounting for Galileo–GPS inter-system biases in precise satellite positioning. *J. Geod.* **2015**, *89*, 81–93. [CrossRef]
15. Tian, Y.; Sui, L.; Xiao, G.; Zhao, D.; Chai, H.; Liu, C. Estimating inter-system biases for tightly combined Galileo/BDS/GPS RTK. *Adv. Space Res.* **2020**, *65*, 572–585. [CrossRef]
16. Zhao, W.; Liu, G.; Gao, M.; Lv, D.; Wang, R. INS-assisted inter-system biases estimation and inter-system ambiguity resolution in a complex environment. *GPS Solut.* **2023**, *27*, 1–13. [CrossRef]
17. Mi, X.; Zhang, B.; Yuan, Y. Multi-GNSS inter-system biases: Estimability analysis and impact on RTK positioning. *GPS Solut.* **2019**, *23*, 1–13. [CrossRef]
18. Zhao, L.; Jiang, J.; Li, L.; Jia, C.; Cheng, J. Characteristics of GPS, BDS2, BDS3 and Galileo inter-system biases and their influence on RTK positioning. *Meas. Sci. Technol.* **2019**, *31*, 015009.
19. Zhao, L.; Jiang, J.; Li, L.; Jia, C.; Cheng, J. High-Accuracy Real-Time Kinematic Positioning with Multiple Rover Receivers Sharing Common Clock. *Remote Sens.* **2021**, *13*, 823. [CrossRef]
20. Zhao, W.; Liu, G.; Gao, M.; Hu, S. Multi-antenna GNSS tight combination attitude determination in the urban environment. *Meas. Sci. Technol.* **2022**, *33*, 065109. [CrossRef]
21. Zeng, A.; Tian, Y.; Chen, X.; Liu, X. Clustering and look-up table calibration of receiver inter-system bias for QZSS and GPS integration. *Meas. Sci. Technol.* **2020**, *31*, 095003. [CrossRef]
22. Tian, Y.; Ge, M.; Neitzel, F.; Zhu, J. Particle filter-based estimation of inter-system phase bias for real-time integer ambiguity resolution. *GPS Solut.* **2017**, *21*, 949–961. [CrossRef]

23. Tian, Y.; Liu, Z.; Ge, M.; Neitzel, F. Multi-dimensional particle filter-based estimation of inter-system phase biases for multi-GNSS real-time integer ambiguity resolution. *J. Geod.* **2019**, *93*, 1073–1087. [CrossRef]
24. Peng, Z.; Gao, C.; Shang, R. Maximum ratio principle-based estimation of difference inter-system bias. *J. Navig.* **2020**, *73*, 1372–1386. [CrossRef]
25. Shang, R.; Gao, C.; Gao, W.; Zhang, R.; Peng, Z.; Liu, Q. Multi-GNSS inter-system model for complex environments based on optimal state estimation. *Meas. Sci. Technol.* **2021**, *32*, 054006. [CrossRef]
26. Dong, D.; Chen, W.; Cai, M.; Zhou, F.; Wang, M.; Yu, C.; Zheng, Z.; Wang, Y. Multi-antenna synchronized global navigation satellite system receiver and its advantages in high-precision positioning applications. *Front. Earth Sci.* **2016**, *10*, 772–783. [CrossRef]
27. Chen, W. A remark on the GNSS single difference model with common clock scheme for attitude determination. *J. Appl. Geod.* **2016**, *10*, 167–173. [CrossRef]
28. Chen, W.; Qin, H.; Zhang, Y.; Tian, J. Accuracy assessment of single and double difference models for the single epoch GPS compass. *Adv. Space Res.* **2012**, *49*, 725–738. [CrossRef]
29. Chen, W.; Yu, C.; Dong, D.; Cai, M.; Zhou, F.; Wang, Z.; Zhang, L.; Zheng, Z. Formal Uncertainty and Dispersion of Single and Double Difference Models for GNSS-Based Attitude Determination. *Sensors* **2017**, *17*, 408. [CrossRef]
30. Schön, S.; Pham, H.K.; Kersten, T.; Leute, J.; Bauch, A. Potential of GPS common clock single-differences for deformation monitoring. *J. Appl. Geod.* **2016**, *10*, 45–52. [CrossRef]
31. Zhang, L.; Hou, Y.; Wu, J. A drift line bias estimator: ARMA-based filter or calibration method, and its application in BDS/GPS based attitude determination. *J. Geod.* **2016**, *90*, 1331–1343.
32. Zhang, C.; Dong, D.; Chen, W.; Cai, M.; Peng, Y.; Yu, C.; Wu, J. High-Accuracy Attitude Determination Using Single-Difference Observables Based on Multi-Antenna GNSS Receiver with a Common Clock. *Remote Sens.* **2021**, *13*, 3977. [CrossRef]
33. Wu, M.; Luo, S.; Wang, W.; Liu, W. Performance Assessment of BDS-2/BDS-3/GPS/Galileo Attitude Determination Based on the Single-Differenced Model with Common-Clock Receivers. *Remote Sens.* **2021**, *13*, 4845. [CrossRef]
34. Keong, J.; Lachapelle, G. Heading and pitch determination using GPS/GLONASS. *GPS Solut.* **2000**, *3*, 26–36. [CrossRef]
35. Li, Y.; Zhang, K.; Roberts, C.; Murata, M. On-the-fly GPS-based attitude determination using single-and double-differenced carrier phase measurements. *GPS Solut.* **2004**, *8*, 93–102. [CrossRef]
36. Macias-Valadez, D.; Santerre, R.; Larochelle, S.; Landry, R. Improving vertical GPS precision with a GPS-over-fiber architecture and real-time relative delay calibration. *GPS Solut.* **2012**, *16*, 449–462. [CrossRef]
37. Wu, M.; He, Y.; Luo, S.; Liu, W. Particle filter-based real-time phase line bias estimation for GNSS-based attitude determination with common-clock receivers. *Adv. Space Res.* **2022**. [CrossRef]
38. Herring, T.A.; King, R.W.; Floyd, M.A.; McClusky, S.C. *GAMIT Reference Manual: GPS Analysis at MIT (Release 10.7)*; Massachusetts Institute of Technology (MIT): Cambridge, MA, USA, 2018. Available online: http://geoweb.mit.edu/gg/GAMIT_Ref.pdf (accessed on 20 August 2022).
39. Teunissen, P.J.G. The least-squares ambiguity decorrelation adjustment: A method for fast GPS integer ambiguity estimation. *J. Geod.* **1995**, *70*, 65–82. [CrossRef]
40. Euler, H.J.; Schaffrin, B. On a Measure for the Discernibility between Different Ambiguity Solutions in the Static-kinematic GPS-mode. In Proceedings of the IAG Symposia, Banff, AL, Canada, 10–13 September 1990.
41. Hofmann-Wellenhof, B.; Lichtenegger, H.; Wasle, E. *GNSS–Global Navigation Satellite Systems: GPS, GLONASS, Galileo, and More*, 1st ed.; Springer: Berlin, Germany, 2007; p. 442.
42. Odolinski, R.; Teunissen, P.J.G.; Odijk, D. First combined COMPASS/BeiDou-2 and GPS positioning results in Australia. Part II: Single- and multiple-frequency single-baseline RTK positioning. *J. Spat. Sci.* **2014**, *59*, 25–46. [CrossRef]